Journal of Power Sources 271 (2014) 114–123

Contents lists available at ScienceDirect

Journal of Power Sources

journal homepage: www.elsevier.com/locate/jpowsour

Lithium-ion battery state of health monitoring and remaining useful life prediction based on support vector regression-particle filter

Hancheng Dong [a, b, *], Xiaoning Jin [b], Yangbing Lou [b], Changhong Wang [a]

[a] Space Control and Inertial Technology Research Center, Harbin Institute of Technology, 2 Yikuang Street, Nangang District, Harbin 150001, China
[b] Department of Mechanical Engineering, University of Michigan, Ann Arbor, MI 48109-2136, United States

HIGHLIGHTS

- Battery State-of-Health is estimated by the health condition parameters.
- Propose capacity degradation parameters to analyze capacity degradation online.
- Propose the RUL prediction model to predict the RUL and update its distribution.
- A novel support vector regression-particle filter algorithm is used in the research.

ARTICLE INFO

Article history:
Received 29 March 2014
Received in revised form
24 July 2014
Accepted 28 July 2014
Available online 6 August 2014

Keywords:
Lithium-ion battery
State-of-health
Capacity degradation parameter
Remaining useful life
RUL prediction model
Support vector regression-particle filter

ABSTRACT

Lithium-ion batteries are used as the main power source in many electronic and electrical devices. In particular, with the growth in battery-powered electric vehicle development, the lithium-ion battery plays a critical role in the reliability of vehicle systems. In order to provide timely maintenance and replacement of battery systems, it is necessary to develop a reliable and accurate battery health diagnostic that takes a prognostic approach. Therefore, this paper focuses on two main methods to determine a battery's health: (1) Battery State-of-Health (SOH) monitoring and (2) Remaining Useful Life (RUL) prediction. Both of these are calculated by using a filter algorithm known as the Support Vector Regression-Particle Filter (SVR-PF). Models for battery SOH monitoring based on SVR-PF are developed with novel capacity degradation parameters introduced to determine battery health in real time. Moreover, the RUL prediction model is proposed, which is able to provide the RUL value and update the RUL probability distribution to the End-of-Life cycle. Results for both methods are presented, showing that the proposed SOH monitoring and RUL prediction methods have good performance and that the SVR-PF has better monitoring and prediction capability than the standard particle filter (PF).

1. Introduction

Lithium-ion batteries are a source for major or supplementary power in many kinds of devices, they are quickly becoming the most common power source for Electric Vehicles (EV) [1]. Remaining Useful Life (RUL) of a battery is defined as the useful life left on the battery at a particular time of operation. RUL estimation is essential to the Condition Based Maintenance (CBM) and health management of the battery [2]. It is important to find a reliable and accurate approach to monitor the Lithium-ion battery State-of-Health (SOH) and predict the RUL, to provide timely maintenance and replacement of the battery system [3–4].

Many studies in the field of Lithium-ion battery health condition estimation are principally based on the development of prognostics tools [5–8]. Regression algorithms such as Support Vector Machine (SVM) [9] and Relevance Vector Machine (RVM) [10] were applied to Lithium-ion battery health condition analysis, which have been able to estimate the degradation trend of battery performance. Meanwhile, Kalman Filters [11–14] were used by some researchers to study battery health due to their capability to estimate the battery state parameters from experimental data. Moreover, a Particle Filter (PF) is able to deal with more general system models than a Kalman Filter, consequently it has also been applied to battery SOH monitoring and RUL prediction [15–18]. The PF estimated value and probability distribution of the RUL are good indicators of Lithium-

* Corresponding author. Space Control and Inertial Technology Research Center, Science Park of Harbin Institute of Technology, Room 303, Building E2, 2 Yikuang Street, Nangang District, Harbin 150001, China Tel.: +86 13796626062.
E-mail addresses: donghancheng85@gmail.com (H. Dong), xnjin@umich.edu (X. Jin), yangbing@umich.edu (Y. Lou), cwang@hit.edu.cn (C. Wang).

http://dx.doi.org/10.1016/j.jpowsour.2014.07.176
0378-7753/

ion battery related maintenance [16–18]. Especially, Saha et al. [17] focused on battery SOH monitoring and RUL prediction by using the battery impedance data extracted from Electrochemical Impedance Spectroscopy (EIS), which provided an approach for the application of the PF in the field of Lithium-ion battery health prognostics. The impedance of Lithium-ion battery provides important data for the estimation of battery degradation [19]. The correlation between the Lithium-ion battery impedance and capacity was observed in several studies [20,21].

In the light of these previous works, the correlation between battery capacity and impedance [20,21] provides new parameters for analyzing the battery capacity degradation. These capacity degradation parameters should be estimated through an online process so the real time battery health condition can be monitored. Similar parameters have been estimated by the linear regression algorithm by Takeno et al. [20].

Moreover, the battery RUL can be predicted by projecting the PF algorithm estimated capacity degradation trend out until the capacity reaches the End of Life (EOL) criterion. The probability distribution parameters at the last time step of online updating are treated as the final RUL distribution [15–18]. However, the RUL prediction is a multi-step ahead prediction process, a few more cycles should be processed after the online updating stops, so the probability distribution parameters of the RUL are not updated when the time step changes.

In this study, a method for battery SOH monitoring is developed to analyze the proposed capacity degradation parameters online and build a novel RUL prediction model which is able to update the RUL probability distribution parameters. Moreover, a Support Vector Regression-Particle Filter (SVR-PF) algorithm is implemented in the research to improve the standard PF against the degeneracy phenomenon. The RUL prediction is based on the SOH monitoring results and the percentage of nominal capacity is used to represent the battery SOH.

The rest of this paper is organized as follows: Section 1 reviewed the related literature and introduced the general content of the paper. Section 2 introduces the basic algorithms of the PF and SVR-PF. Section 3 describes the battery data and the circuit model. In section 4 the estimation of battery health condition parameters and the modeling of the lithium-ion battery are introduced. Section 5 presents the new RUL prediction method. In section 6 the simulation results are shown to test the performance of the proposed SOH monitoring and RUL prediction methods and compare the estimation and prediction capability between the SVR-PF and the standard PF. The conclusions are given lastly in section 7.

2. Particle filter and support vector regression-particle filter

2.1. Particle filter

Particle filter (PF) is a general algorithm based on the recursive Bayesian estimation [22], which uses the Monte Carlo method to draw samples (also called particles) from a posterior distribution and assigns a weight to each particle [23].

Compared to the Kalman Filter which only focuses on linear systems and Gaussian noise [24], a particle filter focuses on a more general situation where the system can be nonlinear and the noise distribution can be non-Gaussian. The system state space model for PF is:

$$\begin{cases} x_k = f(x_{k-1}, v_{k-1}) \\ z_k = h(x_k, n_k) \end{cases} \tag{1}$$

where the system states are represented by x_k, either the measurements or the system outputs is represented by z_k and the system noise and measurement noise are represented by v_{k-1} and n_k respectively, which both can be either Gaussian or non-Gaussian.

Suppose we know the prior distribution $p(x^i_{0:k-1}|z_{1:k-1})$ and have already drawn N samples from the posterior distribution from system (1). The approximation of the posterior distribution is:

$$p(x_{0:k}|z_{1:k}) \approx \sum_{i=1}^{N} w^i_k \delta\left(x_{0:k} - x^i_{0:k}\right) \tag{2}$$

where the samples (i.e., the particles) are represented by $\{x^i_k\}$ and the sample weights are represented by $\{w^i_k\}$ which have $\sum_i^N w^i_k = 1$. A higher weight indicates a higher probability of a sample. $\delta()$ is the Dirac-Delta function.

It is hard to sample directly from a posterior distribution, therefore we use another technique known as Importance Sampling, which draws samples from the importance distribution and has this form:

$$q(x_{0:k}|z_{1:k}) \approx \sum_{i=1}^{N} \delta\left(x_{0:k} - x^i_{0:k}\right) \tag{3}$$

If the importance distribution (3) is substituted into (2), the weight update is given by:

$$w^i_k = \frac{p\left(x^i_{0:k}|z_{1:k}\right)}{q\left(x^i_{0:k}|z_{1:k}\right)} \tag{4}$$

If the importance distribution (3) can be decomposed to:

$$q(x_{0:k}|z_{1:k}) = q(x_k|x_{0:k-1}, z_{1:k}) q(x_{0:k-1}|z_{1:k-1}) \tag{5}$$

We can have the weight renew equation based on Bayesian estimation:

$$\begin{aligned} w^i_k &= \frac{p\left(z_k|x^i_k\right) p\left(x^i_k|x^i_{k-1}\right) p\left(x^i_{0:k-1}|z_{1:k-1}\right)}{q\left(x^i_k|x^i_{0:k-1}, z_{1:k}\right) q\left(x^i_{0:k-1}|z_{1:k-1}\right)} \\ &= w^i_{k-1} \frac{p\left(z_k|x^i_k\right) p\left(x^i_k|x^i_{k-1}\right)}{q\left(x^i_k|x^i_{0:k-1}, z_{1:k}\right)} \end{aligned} \tag{6}$$

where the likelihood function is represented by $p(z_k|x^i_k)$ and the state transfer distribution is represented by $p(x^i_k|x^i_{k-1})$. If system (1) follows the Markov process, the weight renew Equation (6) can be simplified to

$$w^i_k = w^i_{k-1} \frac{p\left(z_k|x^i_k\right) p\left(x^i_k|x^i_{k-1}\right)}{q\left(x^i_k|x^i_{k-1}.z_k\right)} \tag{7}$$

If we choose state transfer distribution to be the importance distribution:

$$q\left(x^i_k|x^i_{k-1}, z_k\right) = p\left(x^i_k|x^i_{k-1}\right) \tag{8}$$

The weight update equation can be simplified to (9) in which the likelihood function $p(z_k|x^i_k)$ and the prior weights are used to update the new weights [25]:

$$w^i_k = w^i_{k-1} p\left(z_k|x^i_k\right) \tag{9}$$

Resampling is used to avoid the problem of degeneracy of the PF algorithm. Without resampling, after a few iterations, some of the

particle weights will tend toward zero and efforts for calculating these weights becomes unnecessary. This condition is known as the degeneracy phenomenon.

To avoid the degeneracy phenomenon, it is standard to remove the small weight particles duplicate large weight particles to renormalize the distribution, and set the weights of all the particles to $1/N$. (N is the number of particles). This is the resampling algorithm of the standard PF.

The threshold of resampling is defined as effective sample N_{eff}, and is calculated by:

$$N_{\text{eff}} = \frac{N}{1+\text{var}\left(w_k^i\right)} \approx \frac{1}{\sum_{i=1}^{N}\left(w_k^i\right)^2} \tag{10}$$

2.2. Support vector regression-particle filter (SVR-PF)

The standard PF algorithm for avoiding the degeneracy phenomenon by eliminating small weight particles and duplicating large weight particles will cause the loss of particle diversity. This will result in most particles gathering around the larger weighted ones, and therefore the degeneracy phenomenon will still exist. In order to avoid this problem, a new resampling algorithm is introduced to rebuild a posterior distribution (2), and is known as SVR [26], which can avoid the degeneracy phenomenon and keep the diversity of particles. The application of the SVR-PF can be found in several studies [27–29].

The fundamental idea that rebuilds posterior distributions by SVR is known as an optimization problem using a regularized functional with constraints [30], which has the following form:

$$\begin{cases} \max W\left(a_i, a_i^*\right) = -\frac{1}{2}\sum_{i=1}^{m}\sum_{j=1}^{m}\left(a_i^* - a_i\right)\left(a_j^* - a_j\right)\left(z_i^T z_j\right) - \sigma_l\sum_{i=1}^{m}\left(a_i^* + a_i\right) + \sum_{i=1}^{m} y_i\left(a_i^* - a_i\right) \\ \text{s.t.}\sum_{i=1}^{m}\left(a_i^* - a_i\right) = 0, 0 \le a_i, a_i^* \le C, i = 1,2,\ldots,m \end{cases} \tag{17}$$

$$\begin{cases} \Omega = (f,f)_H \\ \text{s.t.}\sup_x |F(x) - F_l(x)| = \sup_x \left| F_l(x) - \int_{-\infty}^{x} f(t)\mathrm{d}t \right| = \sigma_l < \varepsilon \end{cases} \tag{11}$$

where $\Omega = (f, f)_H$ is the regularized functional defined in Hilbert space and is generated by σ_l. σ_l is the error or distance between the distribution functions $F(x)$ and its estimation$F_l(x)$. ε is the constraint.

$F(x)$ is the Probability Density Function (PDF) of the estimate distribution $F_l(x)$. We only need to consider points $x_i\,(i = 1,2,\ldots,m)$ in the particle set, thus (11) can be simplified to:

$$\max_i \left| F_l(x) - \int_{-\infty}^{x} f(t)\mathrm{d}t \right|_{x=x_i} = \sigma_l < \varepsilon \tag{12}$$

If the PDF $f(x)$ is described by kernel functions:

$$f(x) = \sum_{i=1}^{m} \beta_i K(x_i, x) \tag{13}$$

$K(x_i,x) = \varphi^T(x_i)\varphi(x)$ is the kernel function which satisfies Mercer's condition. Then we can get the regularized functional:

$$\Omega(f) = (f,f)_H = \sum_{i=1}^{m}\sum_{j=1}^{m}\beta_i\beta_j K(x_i, x_j) \tag{14}$$

The posterior distribution estimation problem can be described as a constraint optimization problem:

$$\begin{cases} \min W_p(\beta) = \sum_{i=1}^{m}\sum_{j=1}^{m}\beta_i\beta_j K(x_i, x_j) \\ \text{s.t.}\max_i \left| F_i(x) - \sum_{j=1}^{m}\beta_j \int_{-\infty}^{x} K(x_j, t)\mathrm{d}t \right|_{x=x_i} = \sigma_l \end{cases} \tag{15}$$

set $y_i = F_i(x_i), w = [\beta_1,\beta_2,\ldots,\beta_m]^T z_j(x) = \int_{-\infty}^{x_j} K(x,t)\mathrm{d}t, z_i = (z_i(x_1), z_i(x_2),\ldots,z_i(x_m))$, ξ_i and ξ_i^* are non-negative slack variables, (15) can be transferred to a quadratic programming problem:

$$\begin{cases} \min J(w,\xi_i,\xi_i^*) = \frac{1}{2}w^T w + C\left(\sum_{i=1}^{m}\xi_i + \sum_{i=1}^{m}\xi_i^*\right) \\ \text{s.t} \quad w^T z_i - y_i \le \sigma_l + \xi_i \\ \qquad y_i - w^T z_i \le \sigma_l + \xi_i^* \\ \qquad \xi_i, \xi_i^* \ge 0, i = 1,2,\ldots m \end{cases} \tag{16}$$

where C is the penalty coefficient. By introducing Lagrange coefficients a_i, a_i^* to (16), we get:

Now the solution of (17) is derived as follows:

$$\beta_j = \sum_{i=1}^{m}\left(a_i^* - a_i\right) z_i(x_j) \tag{18}$$

In (18), the Support Vector is represented by x_i and is the corresponding parameter of non-zero coefficients a_i^*, a_i. Substituting Equation (18) into (13), the solution can be transformed of an optimization problem to a posterior distribution estimation.

From the discussion above, the new PF algorithm can be modified by integrating SVR and can be described as follows: When the effective sample N_{eff} falls below the threshold, a resampling of the posterior distribution using the SVR algorithm occurs. The two training pairs are particle x_k^i and its corresponding weight $w_k^i = F_l(x_k^i)$. These pairs are used to rebuild the resampling posterior distribution. The procedure for the SVR-PF algorithm is shown in Fig. 1.

In Fig. 1, $\tilde{x}_k^1, \ldots, \tilde{x}_k^m$ and $\tilde{w}_k^1, \ldots, \tilde{w}_k^m$ represent the rebuilt particles and weights respectively.

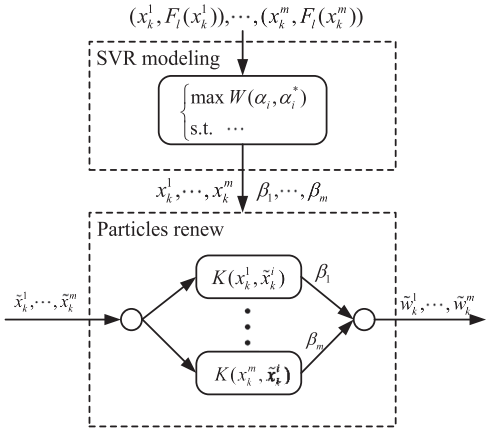

Fig. 1. Fundamental illustration of SVR-PF.

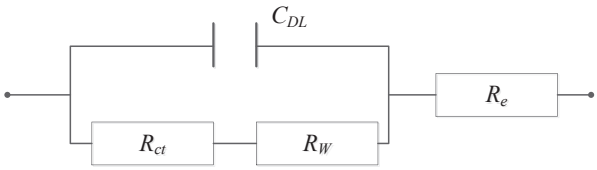

Fig. 2. Equivalent circuit for single cell of battery impedance [31–33].

3. Experimental data and circuit model for the lithium-ion battery

Battery capacity and impedance data are used in this paper, which is collected from the second generation, Gen 2, 18650-size Lithium-ion cells produced by Idaho National Laboratory [31]. The experiment was run at room temperature (24 °C). Charging was carried out in a constant current (CC) mode at 1.5 A until the battery voltage reached 4.2 V and then continued in a constant voltage (CV) mode until the charge current dropped to 20 mA. Discharge was carried out at a CC level of 2 A until the battery voltage fell to 2.7, 2.5 and 2.2 V for batteries 5, 6 and 7 respectively. Impedance measurement was carried out through an EIS frequency sweep from 0.1 Hz to 5 kHz. Repeated charge and discharge cycles resulted in accelerated degradation of the batteries while impedance measurements provided insights into how the internal battery parameters changed. The experiment stopped when the battery reached its EOL threshold. The EOL threshold values for each battery was different. In this experimental study the EOL threshold value for battery 5 and 6 was 70% of nominal capacity; while for battery 7 it was 74.5% nominal capacity.

Impedance data extracted from EIS is a good indicator for determining the battery SOH. When a battery ages, its impedance degrades as a function of time [31,34,35]. Extracted impedance data can be analyzed based on the equivalent circuit for a single cell as shown in Fig. 2. The major impedance data we need for RUL estimation are R_e and R_{ct}, which are mainly contributed by electrolyte and charge transfer. [31].

The battery capacity (Ah) and impedance (Ohm) over cycle number is shown in Fig. 3. Capacity of all three batteries decreased over charge–discharge cycles while the battery impedance R_e and R_{ct} increased over cycles in a similar pattern.

4. Battery SOH monitoring and health condition parameters estimation

In the proposed method, the battery SOH is indicated by health condition parameters: (1) impedance aging parameters [17] provide the impedance aging trend versus time; and (2) capacity degradation parameters reflect battery capacity degradation through the impedance data.

4.1. Model for impedance aging parameter estimation

The time dependent aging of impedance is observed by Refs. [17,31,34,35], and can be modeled by an exponential function:

$$R = R_0 \exp(\lambda_R t) \tag{19}$$

where R represents R_e or R_{ct},R_0 is a constant andλ_R is the impedance aging parameter which is estimated through the PF.

Based on Equation (19), we build a novel battery state space model using the SVR-PF in order to estimate the impedance aging parameters. Besides, the experimental impedance data is also recursively smoothed to reduce the experimental noise interference on the estimation of the capacity degradation parameters:

$$\begin{cases} \lambda_{R,k} = \lambda_{R,k-1} + v_{R,1,k} \\ \tilde{R}_k = \tilde{R}_{k-1} \exp(\lambda_{R,k-1} \Delta k) + v_{R,2,k} \\ R_k = \tilde{R}_k + n_{R,k} \end{cases} \tag{20}$$

where the impedance aging parameter is represented by $\lambda_{R,k}$. The smoothed impedance is represented by $\tilde{R}_k$. The state noise is denoted by $v_{R,1,k}$ and $v_{R,2,k}$. The system measurement R_k represents impedance R_e or R_{ct}. The measurement noise is represented by $n_{R,k}$.

The smoothed impedance $\tilde{R}_k$ is applied to the capacity degradation parameters estimation.

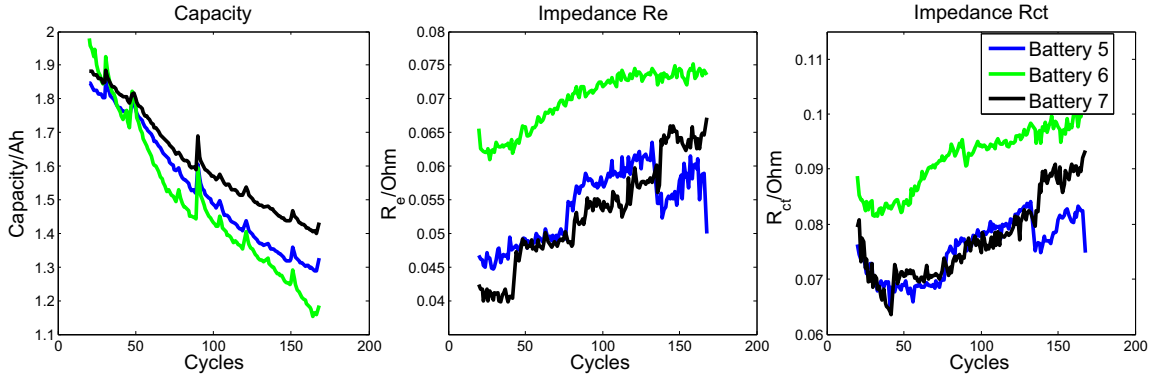

Fig. 3. Battery capacity and impedance versus cycle number [31].

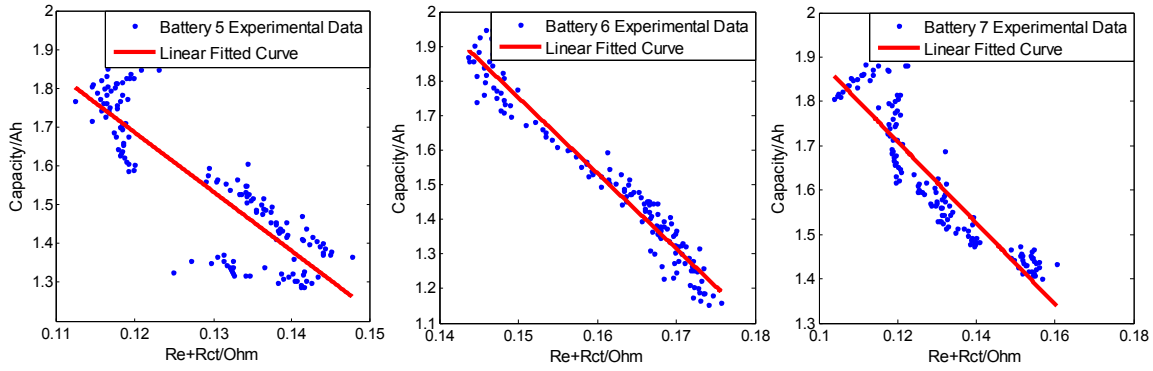

Fig. 4. Illustration of the linear correlation between battery capacity and impedance $R_e + R_{ct}$.

4.2. Capacity degradation model – capacity degradation parameters estimation

Based on the analysis in Refs. [20,21], the capacity degradation is linearly correlated with the sum of the impedance $R_e + R_{ct}$. The correlation is plotted in Fig. 4, and the correlation coefficients of the data are shown in Table 1.

The absolute value of the correlation coefficients of battery capacity and impedance are close to 1, thus they can be modeled by a linear equation:

$$C = \alpha(R_e + R_{ct}) + \beta \tag{21}$$

where the capacity is represented by C, α and β are the capacity degradation parameters.

From Equation (21), the battery capacity degradation model can be determined:

$$\begin{cases} \alpha_k = \alpha_{k-1} + v_{C,1,k-1} \\ \beta_k = \beta_{k-1} + v_{C,2,k-1} \\ C_k = \alpha_k\left(\tilde{R}_{e,k} + \tilde{R}_{ct,k}\right) + \beta_k + n_{C,k} \end{cases} \tag{22}$$

In this model, α_k and β_k are capacity degradation parameters, battery capacity is represented by C_k, $\tilde{R}_{e,k}$ and $\tilde{R}_{ct,k}$ are the smoothed impedance from the model (20). $v_{C,1,k}$, $v_{C,2,k}$ and $n_{C,k}$ are noise.

The battery SOH monitoring stopped when the battery capacity degraded to the RUL threshold. The battery RUL threshold value in this paper is defined as a percentage of the battery nominal capacity, which is greater than the EOL threshold value. The RUL threshold and the EOL threshold have different thresholds criteria: when the RUL threshold criterion was met, the SOH monitoring stopped and the RUL prediction began; the RUL prediction stopped when the EOL thresholds criterion was met and the battery reaches its EOL.

5. Remaining useful life prediction

The prediction of RUL is based on real time battery health condition parameters. When the RUL threshold criterion is met, the SOH monitoring method stops and the current battery health condition parameters are recorded. The impedance is predicted first to provide measurement for the RUL prediction model, the battery capacity is then predicted to calculate the RUL.

The impedance aging parameters are used to predict the impedance. Suppose the RUL threshold criterion is met at cycle N, the battery RUL given in cycle is L and the predicted impedance are given by $\tilde{R}_e$ and $\tilde{R}_{ct}$, we have:

$$\hat{R}_{e,N+m} = \tilde{R}_{e,N}\exp(\lambda_{R_e,N}m).m = 1,\ldots,M.M \geq L \tag{23}$$

$$\hat{R}_{ct,N+m} = \tilde{R}_{ct,N}\exp(\lambda_{R_{ct},N}m).m = 1,\ldots,M.M \geq L \tag{24}$$

In these equations, $\tilde{R}_{e,N}$ and $\tilde{R}_{ct,N}$ are smoothed impedance at cycle N and $\lambda_{R_e,N}$ and $\lambda_{R_{CT},N}$ are estimated impedance parameters at cycle N.

The capacity degradation parameters are embedded in the RUL prediction model which is able to predict the RUL value. The prediction is a multi-step ahead process, causing the estimated particles weights at the last cycle of SOH monitoring to not be able to reflect the distribution of the RUL at the EOL cycle. This model is also built for updating the RUL distribution, and has this form:

Table 1
The correlation coefficients between battery capacity and impedance.

	Battery 5	Battery 6	Battery 7
Coefficients	−0.8699	−0.9661	−0.9157

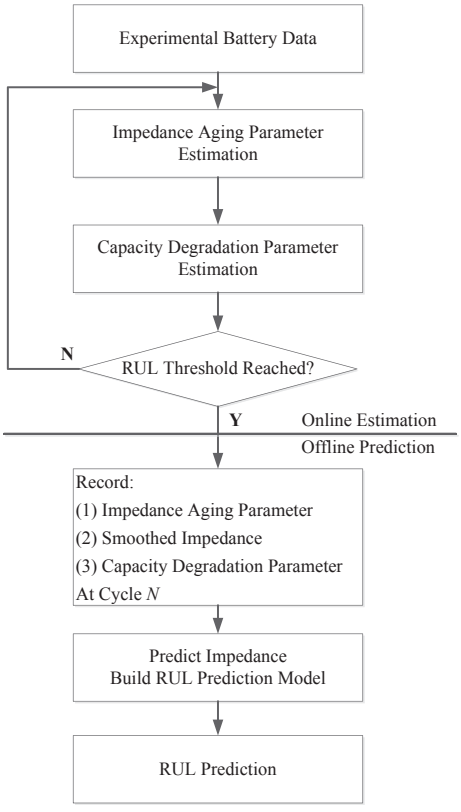

Fig. 5. Flow chart of battery SOH monitoring and RUL prediction.

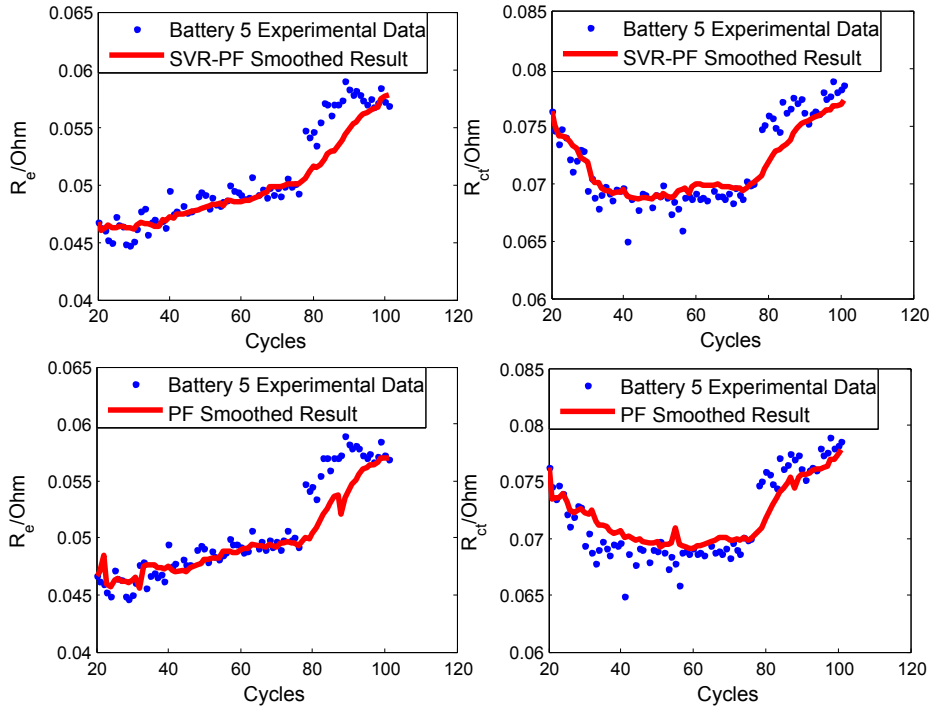

(a) Battery 5

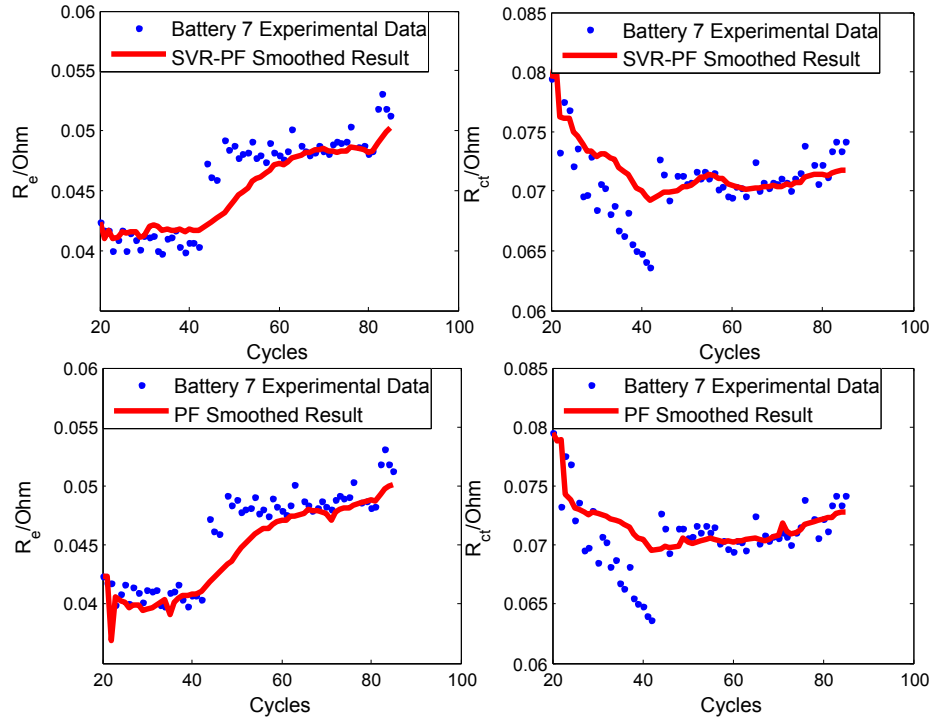

(b) Battery 7

Fig. 6. Battery 5 (a) and battery 7 (b) smoothed results from SVR-PF and PF.

$$
\begin{cases}
\lambda^*_{R_e},k+1=\lambda^*_{R_e},k+v_{a,k}\\
\lambda^*_{R_{\mathrm{ct}}},k+1=\lambda^*_{R_{ct}},k+v_{b,k}\\
R^*_{e,k+1}=R^*_{e,k}\exp\left(\lambda^*_{R_e},k\Delta k\right)+v_{c,k}\\
R^*_{\mathrm{ct},k+1}=R^*_{\mathrm{ct},k}\exp\left(\lambda^*_{R_{\mathrm{ct}}},k\Delta k\right)+v_{d,k}\\
C^*_{k+1}=\alpha_N\left(R^*_{e,k+1}+R^*_{\mathrm{ct},k+1}\right)+\beta_N+v_{e,k}
\end{cases}
\tag{25}
$$

$$
\begin{cases}
\widehat{R}_{e,k}=R^*_{e,k}+n_{a,k}\\
\widehat{R}_{\mathrm{ct},k}=R^*_{\mathrm{ct},k}+n_{b,k}
\end{cases}
$$

In this model, predicted parameters are represented by parameters with *. α_N, β_N are estimated capacity degradation parameters at cycle N. $\widehat{R}_e$ and $\widehat{R}_{\mathrm{ct}}$ are predicted impedance from (23) and (24) respectively. Initial states can be derived at the last cycle of SOH monitoring by using the recursive procedure: $[\lambda_{R_e,N},\lambda_{R_{\mathrm{ct}},N},\tilde{R}_{e,N},\tilde{R}_{\mathrm{ct},N},C_N]^T$. The prediction is started at time step $k=N$ which is the last cycle of the SOH monitoring.

The prediction process stops and the RUL is calculated when the EOL threshold criterion is met. The results provide not only the estimation value, but also the approximate probability distribution.

Table 2
Comparison of the root mean squared errors between SVR-PF and PF data smoothing on battery impedance (Unit: Ohm).

	Battery 5		Battery 7	
	R_e	R_{ct}	R_e	R_{ct}
SVR-PF	1.57×10^{-3}	2.14×10^{-2}	1.75×10^{-3}	2.48×10^{-2}
PF	2.41×10^{-3}	2.53×10^{-2}	2.30×10^{-3}	2.99×10^{-2}

Suppose the EOL threshold is met at cycle N_{EOL}, $\overline{L^*}$ is the predicted RUL, $\{L^{*i}\}$ are the estimated RUL particles which has the number of Q and $\{w^{*i}_{N_{\mathrm{EOL}}}\}$ are the particle weights. The predicted RUL and the RUL distribution are as follows:

$$\overline{L^*} = \sum_{i=1}^{Q} w^{*i}_{N_{\mathrm{EOL}}} L^{*i} = N_{\mathrm{EOL}} - N \tag{26}$$

$$P(L^*) = \sum_{i=1}^{Q} w^{*i}_{N_{\mathrm{EOL}}} \delta\left(L^* - L^{*i}\right) \tag{27}$$

The process of the SOH monitoring and the RUL prediction is diagrammed in Fig. 5.

6. Results

This section evaluates the performance of the proposed SOH monitoring and RUL prediction methods, and also compares the monitoring and prediction capability of the SVR-PF with the standard PF. In order to implement online SOH monitoring and avoid using post-processed data, data from battery 6 is processed beforehand by using a curve fitting algorithm to provide the initial state of the standard PF and the SVR-PF. The experimental data of batteries 5 and 7 is applied in the simulation.

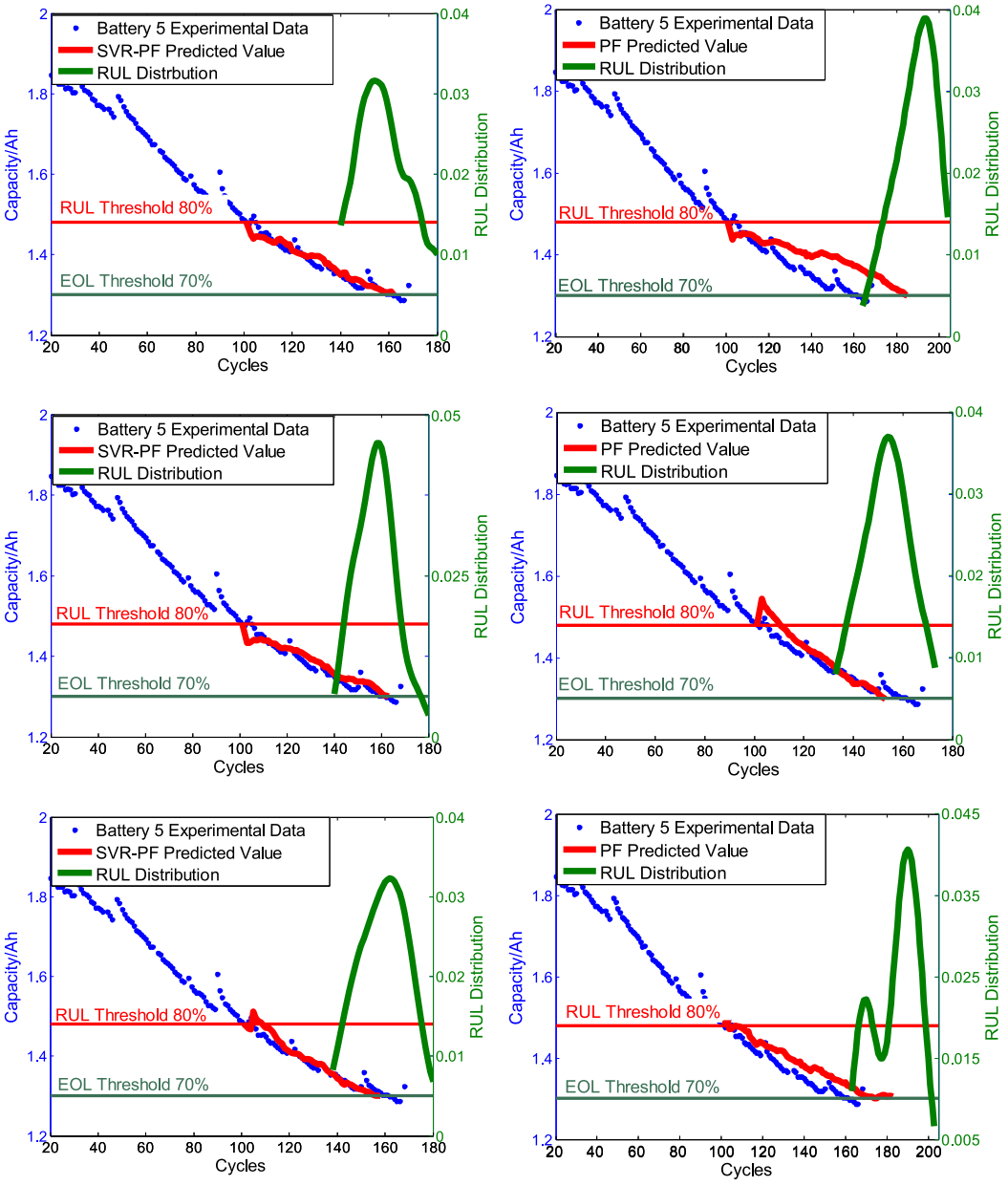

Fig. 7. SVR-PF and PF predicted capacity and RUL distribution of battery 5.

6.1. Battery SOH monitoring

The RUL threshold value of battery 5 was set to 80% nominal capacity and 85% for battery 7. The battery SOH monitoring is calculated by SVR-PF and the standard PF as shown in Fig. 6. The root mean squared errors of the results are shown in Table 2.

By comparing the results from SVR-PF data smoothing with PF data smoothing, SVR-PF is observed to more accurately smooth the data than PF because the root mean squared errors are significantly smaller, as shown in Table 2. Thus the more accurate estimation of the capacity degradation parameters can be calculated by the SVR-PF, which is able to provide a more accurate prediction of the RUL.

6.2. Remaining useful life prediction

We next investigated the battery RUL prediction. The battery 5 RUL threshold value was set to 80% nominal capacity, while 85% for battery 7. The predicted battery capacity and RUL distribution for battery 5 and battery 7 are shown in Figs. 7 and 8. Table 3 shows the predicted value of the EOL and RUL from SVR-PF and standard PF. Random variables were used to generate initial particles and the simulation was repeated three consecutive times.

The results show that the SVR-PF algorithm has robust performance when random initial particles were used and the proposed method of RUL prediction has good results.

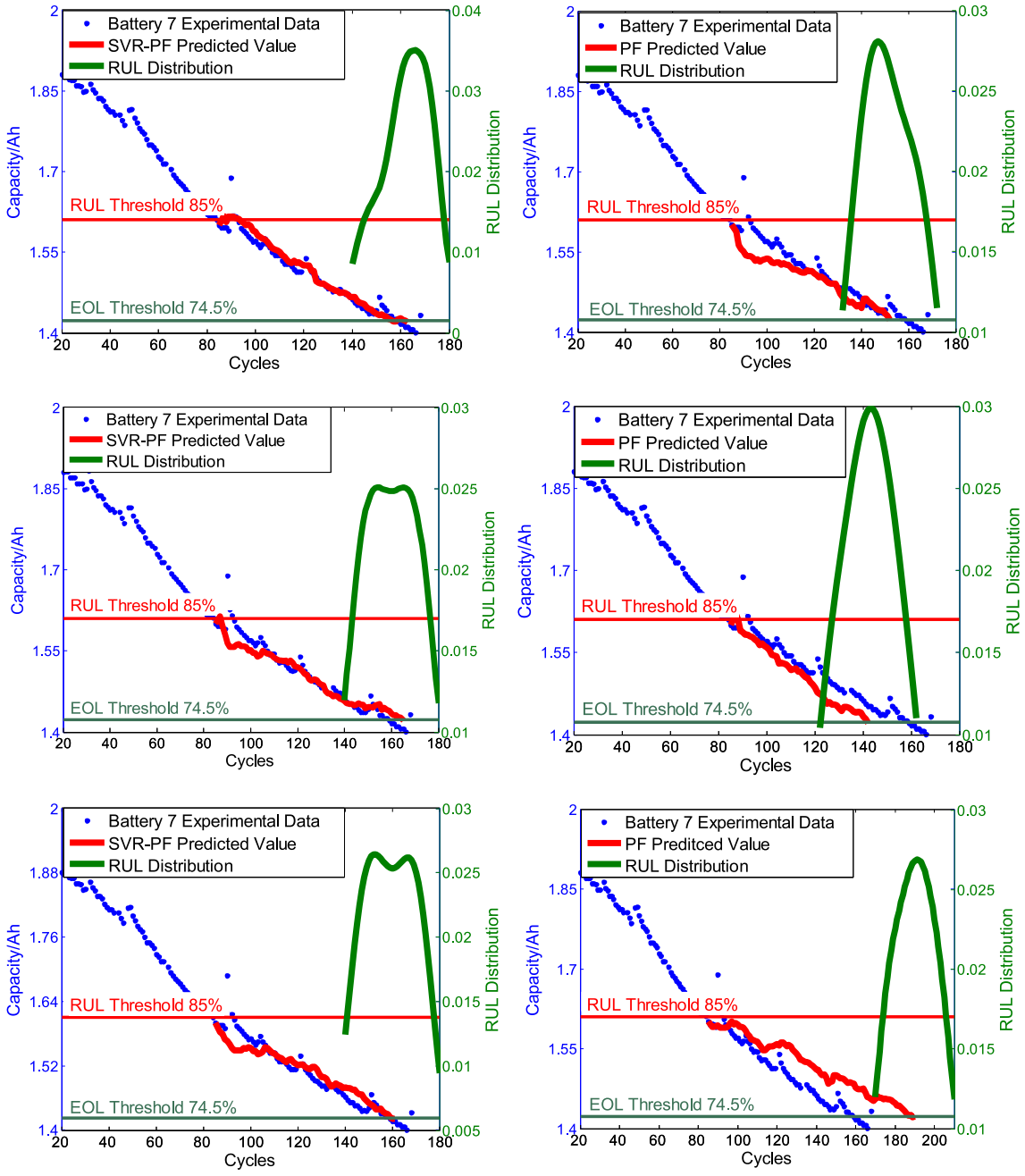

Fig. 8. SVR-PF and PF predicted capacity and RUL distribution of battery 7.

Table 3
Comparison of the predicted RUL and EOL value between SVR-PF and standard PF using three random initial particles (Unit: Cycle).

Simulation labels	Battery 5				Battery 7			
	SVR-PF		PF		SVR-PF		PF	
	RUL	EOL	RUL	EOL	RUL	EOL	RUL	EOL
1	60	161	83	184	78	163	67	152
2	62	163	52	153	80	165	57	142
3	57	158	82	183	76	161	105	190
Measured value	RUL: 61 EOL 162				RUL: 75 EOL: 160			

6.2.1. Effects of RUL threshold value on prediction

In order to study the effect the RUL threshold value has on the prediction performance, the RUL threshold value was changed to 85% of nominal capacity for battery 5 and 90% for battery 7. The prediction results for SVR-PF and standard PF are shown in Fig. 9. The predicted RUL and EOL values are shown in Table 4 with the comparison of the predicted EOL values at the RUL threshold of 80% for battery 5 and 85% for battery 7 in Table 3. (For brevity, only the simulation results with the label number 1 in Table 3 are shown).

In Table 4, the numbers in the brackets are the RUL thresholds values of the prediction. The measured EOL value is represented by EOL (measured).

The increased RUL threshold implies fewer data points are used for prediction, thus the accuracy of RUL prediction will be reduced. However, the prediction results of the proposed SVR-PF method are more accurate than the standard PF method. Moreover, the performance of the standard PF method deteriorated quicker than the SVR-PF method as the number of data points become fewer. Therefore, the SVR-PF algorithm can provide a more robust and accurate prediction of battery RUL.

Table 4
The RUL/EOL predicted value at different RUL thresholds (Unit: Cycle).

	Battery 5			Battery 7		
	RUL (85%)	EOL (85%)	EOL (80%)	RUL (90%)	EOL (90%)	EOL (85%)
SVR-PF	89	168	161	96	162	163
PF	122	201	184	115	181	152
Measured value	RUL (85%): 83 EOL (measured): 162			RUL (90%): 94 EOL (measured): 160		

7. Conclusions

This paper explored improved methods for the Lithium-ion battery SOH monitoring and RUL prediction with the SVR-PF applied. The battery health condition parameters consisted of impedance aging parameters and capacity degradation parameters that were used to estimate the battery SOH. These parameters were then used to build the RUL prediction model after the battery SOH monitoring stopped. Since the SVR-PF algorithm was implemented, the proposed RUL prediction model was able to update the RUL distribution which gave the probability of each possible RUL.

The results showed that the health condition parameters accurately reflected the real time SOH of the battery and ensured that an accurate RUL prediction can be calculated. The accurately predicted RUL value and the updated RUL distribution provide valuable pieces of information necessary for the maintenance decision for the degraded Lithium-ion battery. Moreover, using the experimental data, the robustness of the SVR-PF for battery RUL prognostics was validated, and the SVR-PF showed improved estimation and prediction capability over the standard PF.

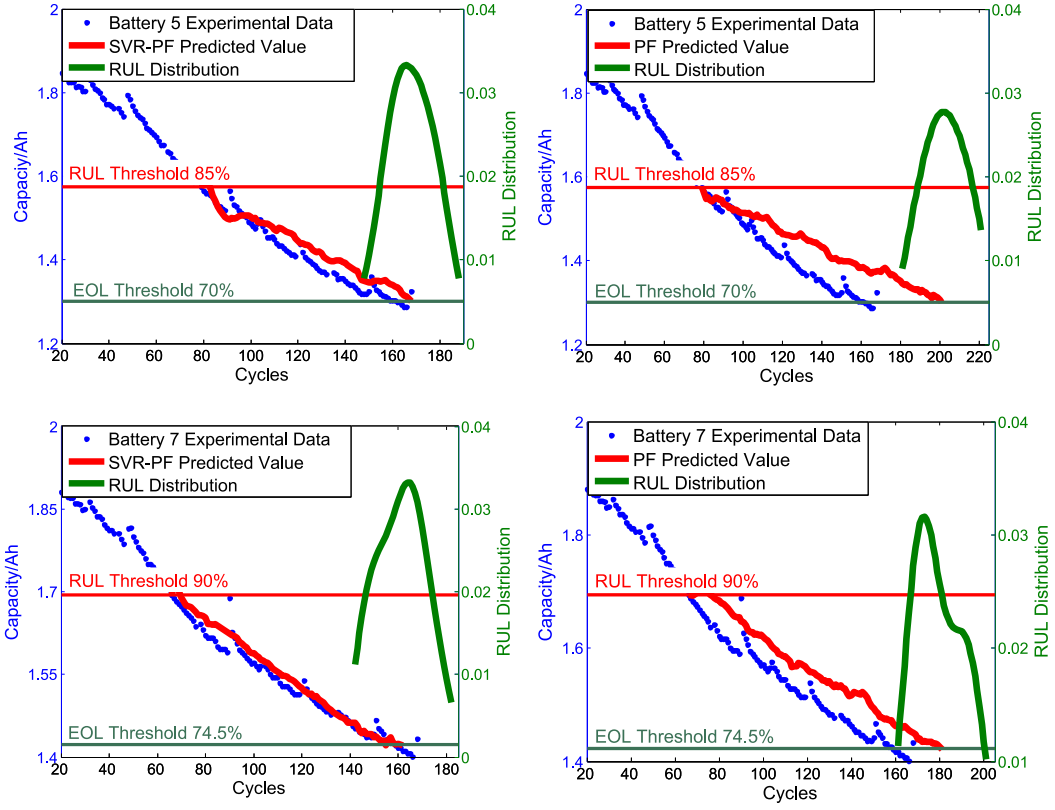

Fig. 9. Effect of the different RUL thresholds on the RUL prediction.

The main contributions of this research can be summarized as: (1) A method for estimating the battery SOH using health condition parameters by SVR-PF was proposed, which has provided a good foundation for multi-step ahead prediction. (2) Battery capacity degradation parameters were extracted to provide accurate RUL predictions together with the impedance aging parameters. (3) A RUL prediction model was proposed to update the RUL probability distribution versus time. (4) The SVR-PF algorithm was used in the study to improve the standard PF against the degeneracy phenomenon.

Future works include the investigation of the physical models for different types of batteries (e.g., Nickel Hydrogen battery) and the integration of the data driven methods with more sophisticated physical based battery models for RUL prediction.

References

[1] Y. Xing, E.W.M. Ma, K.L. Tsui, M. Pecht, Energies 4 (2011) 1840–1857.
[2] X. Si, W. Wang, C. Hu, D. Zhou, Eur. J. Oper. Res. 213 (2011) 1–14.
[3] D. Wang, Q. Miao, M. Pecht, J. Power Sources 239 (2013) 253–264.
[4] A. Eddahech, O. Briat, E. Woirgard, J. Vinassa, Microelectron. Reliab. 52 (2012) 2438–2442.
[5] G. Prasad, C. Rahn, J. Power Sources 232 (2013) 79–85.
[6] Y. Chiang, W. Sean, J. Ke, J. Power Sources 196 (2011) 3921–3932.
[7] Z. Chen, C.C. Mi, Y. Fu, J. Xu, X. Gong, J. Power Sources 240 (2013) 184–192.
[8] A. Schmidt, M. Bitzerb, W. Imre, L. Guzzella, J. Power Sources 195 (2010) 7634–7638.
[9] A. Nuhic, T. Terzimehic, T. Soczka-Guth, M. Buchholz, K. Dietmayer, J. Power Sources 239 (2013) 680–688.
[10] A. Widodo, M. Shim, W. Caesarendra, B. Yang, Expert Syst. Appl. 38 (2011) 11763–11769.
[11] D. Andre, C. Appel, T. Soczka-Guth, D. Sauer, J. Power Sources 224 (2011) 20–27.
[12] G. Plett, J. Power Sources 134 (2004) 252–261.
[13] G. Plett, J. Power Sources 134 (2004) 262–276.
[14] G. Plett, J. Power Sources 134 (2004) 277–292.
[15] J. Liu, W. Wang, F. Ma, Smart Mater. Struct. 20 (2011) 1–9.
[16] W. He, N. Williard, M. Osterman, P. Michael, J. Power Sources 196 (2011) 10314–10321.
[17] B. Saha, K. Goebel, S. Poll, J. Christophersen, IEEE Trans. Instrum. Meas. 58 (2009) 291–296.
[18] Q. Miao, L. Xie, H. Cui, W. Liang, P. Michael, Microelectron. Reliab. 53 (2013) 805–810.
[19] J. Vetter, P. Novak, M.R. Wagner, C. Veit, K.-C. Möller, J.O. Besenhard, M. Winter, M. Wohlfahrt-Mehrens, C. Vogler, A. Hammouche, J. Power Sources 147 (2005) 269–281.
[20] K. Takeno, M. Ichimura, K. Tankano, J. Yamaki, J. Power Sources 128 (2004) 67–75.
[21] R. Jungst, G. Nagasubramanian, H. Case, B.Y. Liaw, A. Urbina, T. Paez, D. Doughty, J. Power Sources 119-121 (2003) 870–873.
[22] H. Sorenson, D. Alspach, Automatica 7 (1971) 465–479.
[23] J. Carpenter, P. Clifford, P. Fearnhead, IEE Proc. Radar, Sonar Navig. 146 (1999) 1–7.
[24] R. Kalman, Trans. ASME J. Basic Eng. 82 (1960) 35–45.
[25] M. Arulampalam, S. Maskell, N. Gordon, T. Clapp, IEEE Trans. Signal Process. 50 (2002) 174–188.
[26] Bishop, Pattern Recognition and Machine Learning, Springer, New York, 2006, pp. 339–344.
[27] W. Jiang, G. Yi, Q. Zeng, IEEE Int. Conf. Intelligent Comput. Intelligent Syst. 1 (2009) 239–243.
[28] N. Kabaoglu, IEEE Trans. Veh. Technol. 58 (2009) 2569–2573.
[29] G. Zhu, D. Liang, Y. Liu, Q. Huang, W. Gao, IEEE Int. Conf. Image Process. 2 (2005). II - 422-5.
[30] V. Vapnik, The Nature of Statistical Learning, Springer, Berlin, 1995, pp. 225–259.
[31] K. Goebel, B. Saha, A. Saxena, J. Celaya, Christophersen, IEEE Instrum. Meas. Mag. 11 (2008) 33–40.
[32] J. Kozlowski, IEEE Aerosp. Conf. Proc. 7 (2003) 3257–3270.
[33] B. Chang, S. Park, Annu. Rev. Anal. Chem. 3 (2010) 207–229.
[34] D. Zhang, B.S. Haran, A. Durairajan, R.E. White, Y. Podrazhansky, B.N. Popov, J. Power Sources 91 (2000) 122–129.
[35] A. Eddahech, O. Briat, N. Bertrand, J. Deletage, J. Vinassa, Int. J. Elec. Power 42 (2012) 487–494.